

Uncovering the Triplet Ground State of Triangular Graphene Nanoflakes Engineered with Atomic Precision on a Metal Surface

Jingcheng Li¹, Sofia Sanz², Jesus Castro-Esteban,³ Manuel Vilas-Varela,³ Niklas Friedrich¹,


Thomas Frederiksen^{2,4,*}, Diego Peña,^{3,†} and Jose Ignacio Pascual^{1,4,‡}

¹*CIC Nanogune BRTA, 20018 Donostia-San Sebastián, Spain*

²*Donostia International Physics Center (DIPC), 20018 Donostia-San Sebastián, Spain*

³*Centro Singular de Investigación en Química Biolóxica e Materiais Moleculares (CiQUS), and Departamento de Química Orgánica, Universidade de Santiago de Compostela, 15705 Santiago de Compostela, Spain*

⁴*Ikerbasque, Basque Foundation for Science, 48013 Bilbao, Spain*

 (Received 16 October 2019; revised manuscript received 17 February 2020; accepted 2 April 2020; published 27 April 2020)

Graphene can develop large magnetic moments in custom-crafted open-shell nanostructures such as triangulene, a triangular piece of graphene with zigzag edges. Current methods of engineering graphene nanosystems on surfaces succeeded in producing atomically precise open-shell structures, but demonstration of their net spin remains elusive to date. Here, we fabricate triangulene-like graphene systems and demonstrate that they possess a spin $S = 1$ ground state. Scanning tunneling spectroscopy identifies the fingerprint of an underscreened $S = 1$ Kondo state on these flakes at low temperatures, signaling the dominant ferromagnetic interactions between two spins. Combined with simulations based on the meanfield Hubbard model, we show that this $S = 1$ π paramagnetism is robust and can be turned into an $S = 1/2$ state by additional H atoms attached to the radical sites. Our results demonstrate that π paramagnetism of high-spin graphene flakes can survive on surfaces, opening the door to study the quantum behavior of interacting π spins in graphene systems.

DOI: 10.1103/PhysRevLett.124.177201

In spite of their apparent simplicity, custom-crafted graphene nanoflakes (GNFs) are predicted to exhibit complex magnetic phenomenology [1] with promising possibilities as active components of a new generation of nanoscale devices [2–4]. As predicted by Lieb’s theorem for bipartite lattices [5], certain shapes of graphene structures may accommodate a spin imbalance in the π electron cloud, resulting in GNFs with a net magnetic moment. Graphene π paramagnetism is more delocalized, mobile, and isotropic than conventional magnetism from d or f states [6] and can be electrically addressed [7,8]. Furthermore, the magnetic moments and their correlations in GNFs can be precisely engineered through their sizes, edge topology, or chemical doping [9–12].

The fabrication of such GNFs has been hindered due to their high reactivity [13]. Because they are open-shell structures, the presence of unpaired electrons (radicals) makes the synthesis difficult. Initially, unsubstituted triangulene was synthesized by dehydrogenating precursor molecules with the tip of a scanning tunneling microscope (STM) [14]. Very recently, triangular GNFs with larger sizes have been synthesized through an on-surface synthetic (OSS) approach [15–17], a strategy for fabricating atomically precise graphene flakes on a metallic surface [18–21]. Despite such progress in fabrication, the magnetic properties of triangular GNFs on a surface have not been demonstrated experimentally.

Here we report the OSS fabrication of triangulene-like GNFs and demonstrate that the GNFs have a triplet ground state. The synthesized GNFs have reduced symmetry compared to triangulene, which increases the localization of the magnetic moments. High-resolution STM images and spectroscopy allow us to identify the two spin centers on the GNFs and map their distribution. Their ferromagnetic correlations are characterized by the spin-1 Kondo effect [22–24], which happens due to the incomplete screening of two coupled spins by conducting electrons of the metal substrate. Our results also show that the strength of correlations between spins depends on the distance between them.

Figure 1(a) shows the chemical structures of the GNF characterized in the experiments, named here extended triangulene (ETRI). This GNF has 19 carbon atoms in one sublattice (highlighted by red circles) and 17 carbon atoms in the other (black circles), which results in a total spin $S = 1$ according to Lieb’s theorem [5]. For comparison, we also produced the GNF in Fig. 1(b) [named as double triangulene (DTRI)], which has 22 carbon atoms in both sublattices and thus a spin $S = 0$ ground state. We synthesized these GNFs by depositing the respective molecular precursors, shown in Figs. 1(c) and 1(d) [details in Supplemental Material (SM) [25]], on a Au(111) surface at 330 °C. The hot surface activates a simultaneous debromination and cyclodehydrogenation step that planarizes them into their final structures.

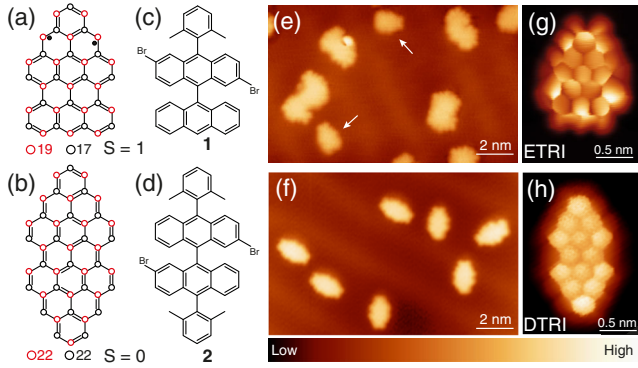


FIG. 1. Chemical structures and synthetic route of extended triangulene and double triangulene. (a), (b) Atomic structures of ETRI and DTRI, which have spin 1 and 0, respectively. Red (black) open circles denote carbon atoms that belong to different sublattices, with the total number of carbon atoms indicated under the structures. (c), (d) Molecular precursors 2,6-dibromo-10-(2,6-dimethylphenyl)-9,9'-bianthracene (precursor 1) and 2,2'-dibromo-10,10'-bis(2,6-dimethylphenyl)-9,9'-bianthracene (precursor 2) used to synthesize ETRI and DTRI, respectively. (e), (f) STM overview images ($V = 0.3$ V, $I = 0.1$ nA) of the formed GNFs from precursors 1 and 2, respectively. The arrows in (e) indicate the ETRI monomers created. (g), (h) Constant height current images ($V = 2$ mV) of ETRI and DTRI with a CO-terminated tip.

Low-temperature STM overview images of the Au (111) surface after deposition of precursors 1 and 2 are shown in Figs. 1(e) and 1(f), respectively. While the reacted precursor 1, ETRI, appears on the surface mostly as monomers and dimers in a ratio of approximately 1:7, nearly all deposited precursors 2, DTRI, remain as monomer species. In every case, the monomers adopt a planar configuration, as expected for the structures in Figs. 1(a) and 1(b). Furthermore, high-resolution STM current images using a CO-terminated tip [34,35] [Figs. 1(g) and 1(h)] reproduce the chemical bond structures of Figs. 1(a) and 1(b), indicating the successful synthesis of ETRI and DTRI. It is worth noting that the current image of DTRI shows merely the backbone structure, as also observed in similar symmetric systems [36], while the current image of ETRI shows additional bright features at the edges. Considering that these images were recorded at 2 mV, the bright features surrounding the backbone structure indicate an enhancement of the local density of states (LDOS) close to Fermi level for the ETRI molecule.

The different shape in the images is better manifested in differential conductance (dI/dV) spectra measured on both types of GNFs [Fig. 2(a)]. The spectrum on ETRI shows a pronounced and narrow (FWHM ~ 1 meV) dI/dV peak centered at zero bias. The zero-bias peak broadens anomalously fast with temperature [as described in Fig. 2(b)] and splits with magnetic fields [Fig. 2(c)], demonstrating that it is a manifestation of the Kondo effect [37]. A (zero-bias) Kondo-derived resonance reflects the screening of a local

spin by conduction electrons [38] and, hence, is a direct proof of the presence of localized magnetic moments on ETRI even when it lies on a metal surface. On the contrary, the spectra taken on DTRI are featureless. Furthermore, both wide-bias range spectra and dI/dV maps reveal their closed-shell ground state (see SM [25]).

The temperature and magnetic field dependence of the Kondo resonances provide further insight on the nature of the spin state of ETRI. Although the Kondo effect is frequently described on $S = 1/2$ systems, it also occurs for higher spin configurations [23,24]. For $S = 1$, a zero-bias resonance reflects a partly screened spin, i.e., with only one interaction channel with the substrate [42]. Similar to the spin-1/2 case, the resonance broadens with temperature [with a Kondo temperature $T_K \sim 6$ K, after Fig. 2(b); see SM [25]] but shows a larger sensitivity to the magnetic field [23,24]. While the Kondo resonance of a $S = 1/2$ system in the strong coupling regime ($T < T_K$) splits linearly with magnetic fields only above a critical field $B_c \geq 0.5k_B T_K / g\mu_b$ [7,43], an underscreened $S = 1$ conserves some magnetic moment, and its zero-bias resonance splits already with $B > 0$ [23,24]. In tunneling spectra, such a peak split should become visible as soon as the Zeeman energy is greater than the thermal broadening ($k_B T$), which, at the 1.2 K of our experimental set up corresponds to fields above 1 Tesla. If the Kondo resonance in Fig. 2(b) were caused by an $S = 1/2$ state, it should appear split in the spectra only for magnetic fields above 3.5 T. However, the peak appears split already at $B = 1.5$ T, proving that the ETRI molecule has an $S = 1$ in an underscreened Kondo state on the gold substrate [25].

The $S = 1$ configuration of the triangular GNFs was further supported by tip-induced manipulation experiments. Because of their biradical character, the zigzag sites show some reactivity and are frequently found passivated by hydrogen atoms produced during the OSS reactions [7,44]. The passivated carbon sites can be identified in high-resolution images by their larger bond length [45] due to the change from sp^2 to sp^3 hybridization. The STM image in Fig. 3(a) shows the bare backbone structure of an ETRI molecule with its characteristic bright features missing due to two additional H atoms passivating the zigzag sites, with its chemical structure shown in Fig. 3(b). The corresponding dI/dV spectrum is featureless around zero bias [black curve in Fig. 3(g)], explaining the absence of bright features in the STM image.

We first cut off one of the passivated H atoms by placing the STM tip on top of site no. 1 in Fig. 3(a) and ramping up the sample bias above 1.5 V [7,44]. The H removal was monitored by a sudden step in the tunneling current [7]. The STM image afterwards appeared with an enhanced LDOS signal around the no. 1 site [Fig. 3(c)], and the dI/dV spectrum on site no. 1 presented a pronounced zero-energy peak [red Fig. 3(g)]. We identify this as $S = 1/2$

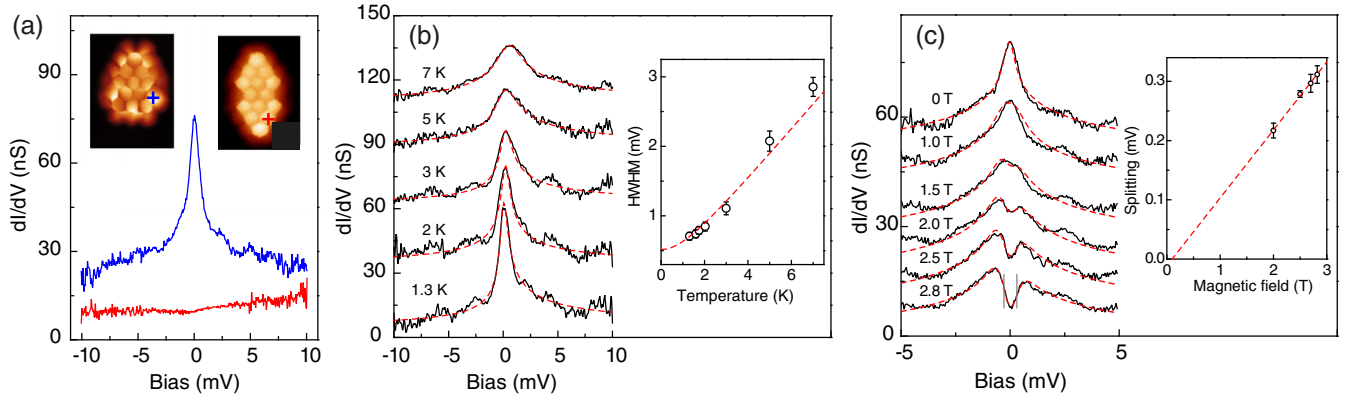


FIG. 2. Kondo resonances in extended triangulene. (a) dI/dV spectra of ETRI (blue curve) and DTRI (red curve) measured at the sites indicated by the colored crosses in the inset. (b) Temperature dependence of the Kondo resonance for an ETRI molecule. The inset plots the half width at half maximum (HWHM) at each temperature, extracted by fitting a Frota function (red dashed lines) [39] and corrected for the thermal broadening of the tip [40]. The plot includes the empirical expression $\sqrt{(\alpha k_B T)^2 + (2k_B T_K)^2}$ [41], fitting the results with $T_K \sim 6$ K and $\alpha = 8.5$. The temperature evolution of the zero-bias conductance, shown as SM [25], agrees with a spin-polarized state in the Kondo regime with energy scale of a few Kelvin. (c) Magnetic field dependence of the Kondo resonance with the field strength indicated in the figure, measured at $T = 1.3$ K. The red dashed lines show the simulated curves using a model for a spin-1 system using the code of Ref. [38]. The inset shows the dependence of Zeeman splitting of the Kondo resonance with magnetic fields, determined from the bias position of steepest slope (indicated on the spectrum at 2.8 T). The dashed line fits the Zeeman splitting with a g factor of 1.98 ± 0.07 . The spectra in (b), (c) are shifted vertically for clarity.

Kondo resonance [7] resulting from the single radical state recovered by the removal of the extra H atom at site no. 1 [Fig. 3(d)]. Following a similar process to cleave the second H-CH bond at site no. 2 recovered bright current features all around the ETRI backbone, resembling the shape of the reference biradical structure of Fig. 1(g). The spectrum

measured again over site no. 1 now shows the Kondo resonance with smaller amplitude and linewidth similar to the one in Fig. 2(a), agreeing with its underscreened $S = 1$ state. As quantified in Fig. 3(h), the Kondo resonance of the doubly dehydrogenated GNFs appeared repetitively with a linewidth of about $\text{HWHM} \sim 0.7$ meV, significantly smaller

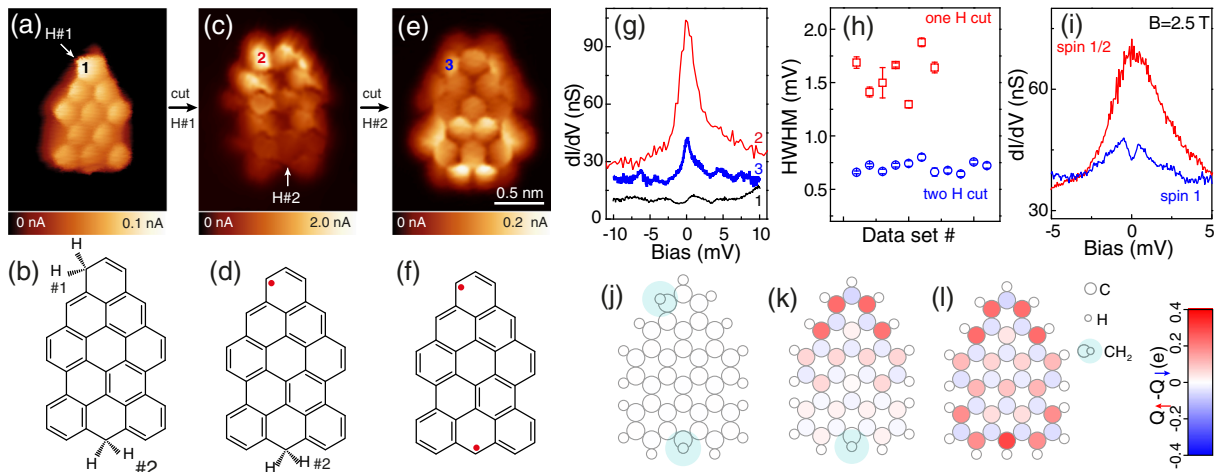


FIG. 3. Spin manipulation by electron-induced removal of extra H atoms. (a) Constant height current image ($V = 2$ mV) of a 2H-ETRI, with its chemical structure shown in (b). (c), (e) Constant height current image ($V = 2$ mV) of the same ETRI of (a) after the electron-induced removal of one and two passivating hydrogen atoms, respectively. The arrows in (a), (c) indicate the STM tip positions during the processes. The corresponding chemical structures are shown in (d), (f). (g) Comparison of dI/dV spectra taken on the three structures at the locations noted with numbers in (a), (c), (e). (h) Comparison of the HWHM from the Kondo resonance taken on 1H-ETRI (red data points) and ETRI (blue data points), respectively. The value of each data point is extracted by fitting the corresponding Kondo resonances with Frota functions [39]. Different data points stand for the measurements from different molecules. (i) Comparison of Kondo resonance taken on 1H-passivated ETRI (red curve) and ETRI (blue curve) at a magnetic field of 2.5 T. (j), (k), (l) Spin polarization of 2H-ETRI, 1H-ETRI, and ETRI from meanfield Hubbard simulations.

than in the singly passivated species hinting at their different Kondo states. The spin assignment of each species was further corroborated by comparing their response to a magnetic field of 2.5 T. While the intermediate $S = 1/2$ specie did not present any detectable split of the Kondo resonance, the biradical one exhibited a clear split, as in Fig. 2(c), demonstrating the larger spin polarization of its $S = 1$ underscreened ground state.

The emergence of magnetism in ETRI is reproduced by both meanfield Hubbard (MFH) and density functional theory (DFT) simulations (see SM [25]). Similar to the case of triangulene [1,46], this modified GNF presents two (singly occupied) zero-energy modes, with a triplet ground state clearly preferred over a singlet one by more than 60 meV (see Figs. S9 and S16). The spin polarization [Fig. 3(l)] shows two spin centers localized at opposite sides of the triangular GNF, with a distribution that resembles the experimental current maps [Figs. 1(g) and 3(e)]. We note that their ferromagnetic exchange interaction is much larger than the Kondo energy scale ($k_B T_K < 1$ meV), thus explaining the $S = 1$ underscreened Kondo ground state found in the experiments. MFH simulations also show that hydrogen passivation of the radical states quenches the spins sequentially, turning ETRI into an $S = 1/2$ doublet [Fig. 3(k)] or completely non-magnetic [Fig. 3(j)], as demonstrated by the electron-induced removal of extra H atoms in the experiments.

A paramagnetic ground state was also found on molecular dimers formed during the OSS process [as shown in Fig. 1(e)], but their larger size crucially affects their magnetic properties. Fig. 4(a) shows a high-resolution image of a dimer. Two ETRI moieties are covalently linked together [Fig. 4(b)] following the Ullmann-like C-C coupling of their halogenated sites [47]. During the cyclo-dehydrogenation step, an extra pentagonal ring is created between them, as highlighted by a red bond in Fig. 4(b), reducing the number of radicals of the dimer to only two. The biradical state is experimentally demonstrated in the SM [25].

The STM image of Fig. 4(a) also reproduces bright features around the dimer backbone (indicated with dashed ellipses) corresponding to the localization of the Kondo effect: dI/dV spectra measured on either of the two show pronounced peaks centered at zero bias [Fig. 4(c)], which broaden with temperature [Fig. 4(d)] and magnetic field [Fig. 4(e)]. However, these Kondo resonances broaden faster with T than for the $S = 1$ case of ETRI [both compared in the inset of Fig. 4(d)] and show no split at $B = 2.7$ T, signaling a different magnetic ground state.

Our MFH simulations of ETRI dimers like in Fig. 4(b) confirm their biradical state, but the energy between triplet and singlet solutions are now closer (see SM). On a surface, a magnetic ground state probably behaves as two noninteracting $S = 1/2$ spins. This explains the lack of B -induced split and the faster broadening with T expected

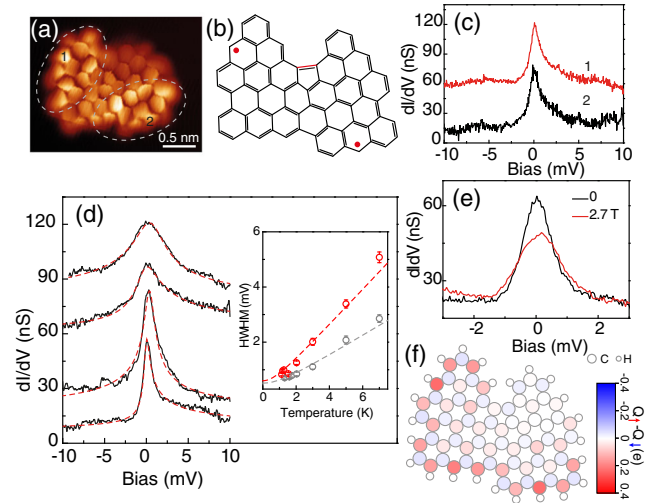


FIG. 4. Magnetic properties of dimers of ETRI. (a) Constant height current image ($V = 2$ mV) of a ETRI dimer with its chemical structure shown in (b). (c) dI/dV spectra taken on the dimer on the sites indicated with corresponding numbers in (a). (d) Temperature dependence of the Kondo resonance taken at site no.2. The spectra are shifted vertically for clarity. The inset plots the HWHM at each temperature, extracted by fitting a Frota function (red dashed lines) [39] and corrected for the thermal broadening of the tip [40]. The inset includes the simulation with the empirical expression $\sqrt{(ak_B T)^2 + (2k_B T_K)^2}$ [41], fitting the results with $T_K \sim 7$ K with $\alpha = 15$. For comparison, the temperature dependence of HWHM from the Kondo resonance taken on a single ETRI monomer (gray data points) is also shown. (e) Kondo resonance taken at location 2 at different magnetic fields at $T = 1.3$ K. (f) Spin polarization of a ETRI dimer from MFH simulations.

for $S = 1/2$ Kondo systems [24]. The spin polarization maps obtained from MFH simulations reproduce the bright current regions on the dimers well [Fig. 4(f)], further corroborating that this signal can be associated to the spin distribution. The origin of such a small magnetic exchange between the two radical states is related to the presence of a pentagon between them and to the larger separation between the two spin centers. In fact, in the absence of this extra C-C bond, MFH simulations find a robust $S = 2$ ground state. Thus, pentagonal rings embedded in certain sites of an open-shell GNF can affect its magnetic state critically by quenching a radical state and modifying the total spin (here by $\Delta S = 1$) [48], just as extra hydrogen atoms do [7], but their placement on a specific site can be designed precisely during the OSS process.

In summary, we have demonstrated the magnetic ground state of graphene flakes fabricated deterministically with a triangularlike shape. The survival of the $S = 1$ state on the metal surface is identified first through the observation of a narrow Kondo resonance, that reacts to magnetic fields as an underscreened spin triplet. The $S = 1$ state was further confirmed through removal of hydrogen atoms by tip

manipulation experiments, which revealed the stepwise emergence of two spins localized at different sides of the flakes. We note that our findings here contrast with the absence of magnetic signals in previous studies of larger triangulene flakes [15,16]. It is therefore an interesting subject for future work to unveil the precise interplay between size and symmetry of GNFs for their magnetic state over a metal surface. Nevertheless, the existence of GNFs with a net spin on a surface opens the door to new investigations of their spin dynamics and coherence over inorganic supports, which are crucial aspects for utilizing graphene nanosystems [49] in quantum spintronic applications.

We are indebted to Carmen Rubio for fruitful discussions. We acknowledge financial support from Spanish AEI (MAT2016-78293-C6, FIS2017-83780-P, and the Maria de Maeztu Units of Excellence Programme MDM-2016-0618), the European Union's Horizon 2020 (FET-Open project SPRING Grant No. 863098), the Basque Departamento de Educación through the Ph.D. Fellowship No. PRE_2019_2_0218 (S. S.), the Xunta de Galicia (Centro singular de investigación de Galicia accreditation, ED431G/09), and the European Regional Development Fund.

*thomas_frederiksen@ehu.es

†diego.pena@usc.es

‡j.pascual@nanogune.eu

- [1] O. V. Yazyev, *Rep. Prog. Phys.* **73**, 056501 (2010).
- [2] W. L. Wang, O. V. Yazyev, S. Meng, and E. Kaxiras, *Phys. Rev. Lett.* **102**, 157201 (2009).
- [3] W. Han, R. K. Kawakami, M. Gmitra, and J. Fabian, *Nat. Nanotechnol.* **9**, 794 (2014).
- [4] Z. Bullard, E. C. Girão, J. R. Owens, W. A. Shelton, and V. Meunier, *Sci. Rep.* **5**, 7634 (2015).
- [5] E. H. Lieb, *Phys. Rev. Lett.* **62**, 1201 (1989).
- [6] B. Trauzettel, D. V. Bulaev, D. Loss, and G. Burkard, *Nat. Phys.* **3**, 192 (2007).
- [7] J. Li, S. Sanz, M. Corso, D. J. Choi, D. Peña, T. Frederiksen, and J. I. Pascual, *Nat. Commun.* **10**, 200 (2019).
- [8] S. Mishra, D. Beyer, K. Eimre, S. Kezilebieke, R. Berger, O. Gröning, C. A. Pignedoli, K. Müllen, P. Liljeroth, P. Ruffieux, X. Feng, and R. Fasel, *Nat. Nanotechnol.* **15**, 22 (2020).
- [9] J. Fernández-Rossier and J. J. Palacios, *Phys. Rev. Lett.* **99**, 177204 (2007).
- [10] W. L. Wang, S. Meng, and E. Kaxiras, *Nano Lett.* **8**, 241 (2008).
- [11] E. Kan, W. Hu, C. Xiao, R. Lu, K. Deng, J. Yang, and H. Su, *J. Am. Chem. Soc.* **134**, 5718 (2012).
- [12] M. E. Sandoval-Salinas, A. Carreras, and D. Casanova, *Phys. Chem. Chem. Phys.* **21**, 9069 (2019).
- [13] E. Clar and D. G. Stewart, *J. Am. Chem. Soc.* **75**, 2667 (1953).
- [14] N. Pavliček, A. Mistry, Z. Majzik, N. Moll, G. Meyer, D. J. Fox, and L. Gross, *Nat. Nanotechnol.* **12**, 308 (2017).
- [15] S. Mishra, D. Beyer, K. Eimre, J. Liu, R. Berger, O. Gröning, C. A. Pignedoli, K. Müllen, R. Fasel, X. Feng, and P. Ruffieux, *J. Am. Chem. Soc.* **141**, 10621 (2019).
- [16] J. Su, M. Telychko, P. Hu, G. Macam, P. Mutombo, H. Zhang, Y. Bao, F. Cheng, Z.-Q. Huang, Z. Qiu, S. J. R. Tan, H. Lin, P. Jelínek, F.-C. Chuang, J. Wu, and J. Lu, *Sci. Adv.* **5**, eaav7717 (2019).
- [17] S. Mishra, D. Beyer, K. Eimre, R. Ortiz, J. Fernández-Rossier, R. Berger, O. Gröning, C. A. Pignedoli, R. Fasel, X. Feng, and P. Ruffieux, [arXiv:2003.00753](https://arxiv.org/abs/2003.00753).
- [18] J. Cai, P. Ruffieux, R. Jaafar, M. Bieri, T. Braun, S. Blankenburg, M. Muoth, A. P. Seitsonen, M. Saleh, X. Feng, K. Müllen, and R. Fasel, *Nature (London)* **466**, 470 (2010).
- [19] M. Treier, C. A. Pignedoli, T. Laino, R. Rieger, K. Müllen, D. Passerone, and R. Fasel, *Nat. Chem.* **3**, 61 (2011).
- [20] P. Ruffieux, S. Wang, B. Yang, C. Sánchez-Sánchez, J. Liu, T. Dienel, L. Talirz, P. Shinde, C. A. Pignedoli, D. Passerone, T. Dumslaff, X. Feng, K. Müllen, and R. Fasel, *Nature (London)* **531**, 489 (2016).
- [21] S. Clair and D. G. de Oteyza, *Chem. Rev.* **119**, 4717 (2019).
- [22] S. Sasaki, S. De Franceschi, J. M. Elzerman, W. G. van der Wiel, M. Eto, S. Tarucha, and L. P. Kouwenhoven, *Nature (London)* **405**, 764 (2000).
- [23] N. Roch, S. Florens, T. A. Costi, W. Wernsdorfer, and F. Balestro, *Phys. Rev. Lett.* **103**, 197202 (2009).
- [24] J. J. Parks, A. R. Champagne, T. A. Costi, W. W. Shum, A. N. Pasupathy, E. Neuscamman, S. Flores-Torres, P. S. Cornaglia, A. A. Aligia, C. A. Balseiro, G. K. L. Chan, H. D. Abruña, and D. C. Ralph, *Science* **328**, 1370 (2010).
- [25] See Supplemental Material at <http://link.aps.org/supplemental/10.1103/PhysRevLett.124.177201> for synthesis and methods details, and for complementary experimental results and simulations, which includes Refs. [24–31].
- [26] Y. Hancock, A. Uppstu, K. Saloriutta, A. Harju, and M. J. Puska, *Phys. Rev. B* **81**, 245402 (2010).
- [27] N. Papior, *sisl: v0.9.6* (2019).
- [28] Y. Hirshberg and E. Fischer, *J. Chem. Soc.* 629 (1953).
- [29] D. Goldhaber-Gordon, J. Göres, M. A. Kastner, H. Shtrikman, D. Mahalu, and U. Meirav, *Phys. Rev. Lett.* **81**, 5225 (1998).
- [30] D. P. Daroca, P. Roura-Bas, and A. A. Aligia, *Phys. Rev. B* **98**, 245406 (2018).
- [31] R. Ortiz, N. A. García-Martínez, J. L. Lado, and J. Fernández-Rossier, *Phys. Rev. B* **97**, 195425 (2018).
- [32] J. M. Soler, E. Artacho, J. D. Gale, A. García, J. Junquera, P. Ordejón, and D. Sánchez-Portal, *J. Phys. Condens. Matter* **14**, 2745 (2002).
- [33] J. P. Perdew, K. Burke, and M. Ernzerhof, *Phys. Rev. Lett.* **77**, 3865 (1996).
- [34] L. Gross, F. Mohn, N. Moll, P. Liljeroth, and G. Meyer, *Science* **325**, 1110 (2009).
- [35] G. Kichin, C. Weiss, C. Wagner, F. S. Tautz, and R. Temirov, *J. Am. Chem. Soc.* **133**, 16847 (2011).
- [36] D. Beyer, S. Wang, C. A. Pignedoli, J. Melidonie, B. Yuan, C. Li, J. Wilhelm, P. Ruffieux, R. Berger, K. Müllen, R. Fasel, and X. Feng, *J. Am. Chem. Soc.* **141**, 2843 (2019).
- [37] M. Ternes, A. J. Heinrich, and W.-D. Schneider, *J. Phys. Condens. Matter* **21**, 053001 (2009).
- [38] M. Ternes, *New J. Phys.* **17**, 063016 (2015).
- [39] H. O. Frota, *Phys. Rev. B* **45**, 1096 (1992).

- [40] Y.-H. Zhang, S. Kahle, T. Herden, C. Stroh, M. Mayor, U. Schlickum, M. Ternes, P. Wahl, and K. Kern, *Nat. Commun.* **4**, 2110 (2013).
- [41] K. Nagaoka, T. Jamneala, M. Grobis, and M. F. Crommie, *Phys. Rev. Lett.* **88**, 077205 (2002).
- [42] M. Pustilnik and L. I. Glazman, *Phys. Rev. Lett.* **87**, 216601 (2001).
- [43] T. A. Costi, *Phys. Rev. Lett.* **85**, 1504 (2000).
- [44] L. Talirz, H. Söde, J. Cai, P. Ruffieux, S. Blankenburg, R. Jafaar, R. Berger, X. Feng, K. Müllen, D. Passerone, R. Fasel, and C. A. Pignedoli, *J. Am. Chem. Soc.* **135**, 2060 (2013).
- [45] L. Gross, F. Mohn, N. Moll, B. Schuler, A. Criado, E. Guitián, D. Peña, A. Gourdon, and G. Meyer, *Science* **337**, 1326 (2012).
- [46] R. Ortiz, R. Á. Boto, N. García-Martínez, J. C. Sancho-García, M. Melle-Franco, and J. Fernández-Rossier, *Nano Lett.* **19**, 5991 (2019).
- [47] D. G. De Oteyza, A. García-Lekue, M. Vilas-Varela, N. Merino-Díez, E. Carbonell-Sanromà, M. Corso, G. Vasseur, C. Rogero, E. Guitián, J. I. Pascual, J. E. Ortega, Y. Wakayama, and D. Peña, *ACS Nano* **10**, 9000 (2016).
- [48] S. Mishra, D. Beyer, R. Berger, J. Liu, O. Gröning, J. I. Urgel, K. Müllen, P. Ruffieux, X. Feng, and R. Fasel, *J. Am. Chem. Soc.* **142**, 1147 (2020).
- [49] F. Lombardi, A. Lodi, J. Ma, J. Liu, M. Slota, A. Narita, W. K. Myers, K. Müllen, X. Feng, and L. Bogani, *Science* **366**, 1107 (2019).